Experimental Study of Two-Fluid Effect during Magnetic Reconnection in the UTST Merging Experiment*)

Kotaro YAMASAKI, Shuji KAMIO[1)], Koichiro TAKEMURA, Qinghong CAO, Takenori G. WATANABE, Hirotomo ITAGAKI, Takuma YAMADA[2)], Michiaki INOMOTO and Yasushi ONO

The University of Tokyo, Kashiwa 277-8561, Japan
[1)]*National Institute for Fusion Science, 322-6 Oroshi-cho, Toki 509-5292, Japan*
[2)]*Faculty of Arts and Science, Kyushu University, 744 Motooka, Nishi-ku, Fukuoka 819-0395, Japan*

(Received 8 December 2012 / Accepted 17 July 2013)

Radial profile of floating potential inside the current sheet was measured for the purpose of investigating the two-fluid (Hall) effect during magnetic reconnection in the UTST merging experiment. During magnetic reconnection, the floating potential drop was formed spontaneously inside the current sheet, forming a steep electric potential gradient on its both downstream areas. Magnetic probe array measurement indicates that this potential drop appears spontaneously when the reconnection rate rapidly increase due to change in current sheet structure. The IDS probe measurement observed outflow almost equal to poloidal Alfvén speed in radial direction from the X-point, where steep gradient of floating potential is formed. This fact suggests that ion acceleration/heating is caused by the steep potential gradient formed in the downstream by magnetized electrons.

Keywords: magnetic reconnection, spherical tokamak, plasma merging, two-fluid effect

DOI: 10.1585/pfr.8.2401130

1. Introduction

The spherical tokamak (ST) is a promissing candidate for core plasma confinement method of fusion reactor for the following features.

- High-β value is achievable (~50%).
- Contain near-omnigenious region, which shows improved confinement in bad curvature region [1].
- Low cost in construction and operation.

However, because of the small aspect ratio ($A < 2$), there would be no room for setting up center solenoid (CS) inside the plasma. Therefore, many methods are being studied to achieve CS-less startup of ST, such as the radio frequency (RF) startup, coaxial helicity injection (CHI) and merging startup.

The merging startup uses the external poloidal field (PF) coils to form two ST plasmas without the CS. In merging startup, two small tokamaks are formed and merged to form one ST. During the ST formation, electrons and ions are heated by an energy conversion process of magnetic reconnection. This starup method has been used firstly by TS-3 (the University of Tokyo), then by START (UKAEA) [2] and recently by TS-4, MAST and UTST. 2D Doppler spectroscopy measured the ion temperature during merging startup in TS-3. In this experiment, ions are heated from 10 eV to 40 - 60 eV within 10 μsec, which corresponds to heating power of as large as 4 - 6 MW [3]. In the merging experiment in MAST, electron and ion temperatures were measured by the Thomson scattering system and neutral particle analyzer, respectively. They indicate that both electrons and ions are heated up to 1 keV after merging. Precise electron temperature measurement was also implemented in MAST [4] and showed strong electron heating at the X-point.

It is noted that the current sheet has higher ion temperature than the inflow region. Our experiment indicates the reconnection outflow as a the major heating mechanism, but needs a modification in the two-fluid regime. This paper addresses the first experimental observation of electrostatic potential drop due to the two fluid effects and its heating effect.

2. The UTST Plasma Merging Device

The merging startup ST device, UTST, is designed to examine the feasibility of merging startup for fusion reactors. The cross-section of UTST is shown in Fig. 1. Unlike START/MAST and TS-3/TS-4, all coils are placed outside the vacuum vessel. In the UTST merging startup experiment, PF#2,4 coil currents are swung to induce electric field in toroidal direction for initial formation of two ST. After the initial tokamaks are formed, PF#1 coil current compress and merges them at the midplane of the vacuum vessel. With this startup method, we have produced successfully the maximum plasma current of 60 kA without

author's e-mail: yamasaki@ts.t.u-tokyo.ac.jp
*) This article is based on the presentation at the 22nd International Toki Conference (ITC22).

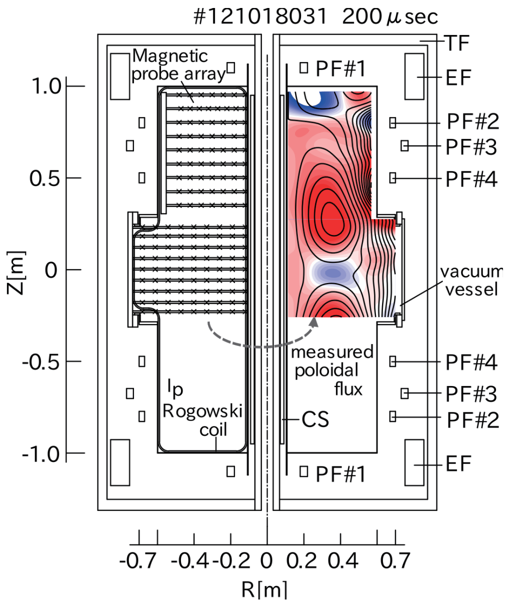

Fig. 1 Cross section diagram of UTST. Coil position, magnetic probe distribution, and Ip Rogowski coil layout are shown. Line and color contours show poloidal flux and toroidal current density of typical discharge calculated from magnetic probe array signals.

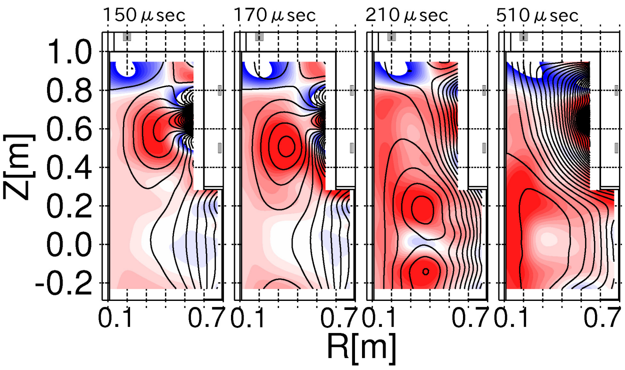

Fig. 2 Time evolution of poloidal flux (line contour) with toroidal current density (color contour) of typical discharge.

CS assist.

The typical merging startup is shown in Fig. 2. Line and color contour plot on Figs. 1 and 2 indicate poloidal flux ψ and toroidal current density j_t, respectively. These values are calculated from the magnetic field measurement with a magnetic probe array placed inside the vacuum vessel, as shown in Fig. 1. Magnetic probe array measures toroidal and axial components of the magnetic field. Poloidal flux ψ, toroidal current density j_t and toroidal electric field E_t are calcurated as follows,

$$\psi(R)=2\pi \int_0^R R' B_z dR', \tag{1}$$

$$E_t(R)= -\frac{1}{2\pi R} \left.\frac{d\psi}{dt}\right|_{R'=R}, \tag{2}$$

$$j_t(R)= -\frac{1}{\mu_0}\left[\frac{dB_r}{dz} - \frac{dB_z}{dR'}\right]_{R'=R} = -\frac{1}{\mu_0}\left[\frac{1}{2\pi R'}\frac{d^2\psi}{dz^2} - \frac{dB_z}{dR'}\right]_{R'=R}. \tag{3}$$

3. Two-Fluid Effect On Magnetic Reconnection

Magnetic reconnection has been mainly described by resistive MHD model. In this model, the diffusion by collisional resistivity is the cause for field-line reconnection. Since both of ion gyro-radius $\rho_i \sim 79$ mm and the mean free path $\lambda_{mfp} \sim 120$ mm are longer than thickness of sheet current $\delta \sim 50$ mm, ideal MHD interpretation of reconnection needs some modification. In such a situation, electron and ion must behave independently inside the current sheet. The MHD interpretation of reconnection should be modified by these effect such as Hall effect [5].

In this paper, we address the first experimental observation of ion acceleration/heating caused by electron potential that magnetized electrons form during magnetic reconnection.

4. Diagnostics

To see the two-fluid effect inside the current sheet, an electrostatic probe was inserted to measure the radial profile of floating potential. The floating potential ϕ_f is a kind of electric potential where ion current and electron currents balance. ϕ_f is defined as follows;

$$\phi_f = \phi_s + \frac{\kappa T_e}{e}\left[\ln\left(\frac{Z_i n_i}{n_e}\sqrt{\frac{m_e}{m_i}}\right) - \frac{1}{2}\right], \tag{4}$$

where ϕ_s is the space potential T_e is the electron temperature, Z is the ion charge number and $n_{i,e}$ are ion/electron density. As shown in eq. 4, ϕ_f is proportional to T_e, the floating potential difference can be, approximately, considered as electrostatic potential difference, given that spatial difference of T_e is sufficiently small. An ion Doppler spectroscopy (IDS) probe was also inserted for ion velocity/temperature measurement. Figure 3 shows these probe locations. The electrostatic probe is mainly composed of ϕ10 mm glass tube with ϕ1 mm tungsten tip, which is inserted into plasma by 5 mm. A linear isolation amplifier (ACPL-7900) is used to reduce the common mode noise and insulation between the plasma and digitizer.

The IDS probe consists of optical lens and collimater attached at the head of ϕ5 glass shaft with a quartz fiber inside it to gather and transmit ion emission to the detector. In UTST, He II line (468.58 nm) emission localized around the X-point was already measured during magnetic reconnection [6]. Since C III line (464.74 nm) emission is also detected at almost the same time and location as the He II line emission, C III line is used for ion flow velocity and temperature measurement.

We made a radial scan of this probe for measuring the spatial profiles of floating potential, ion flow velocity, and

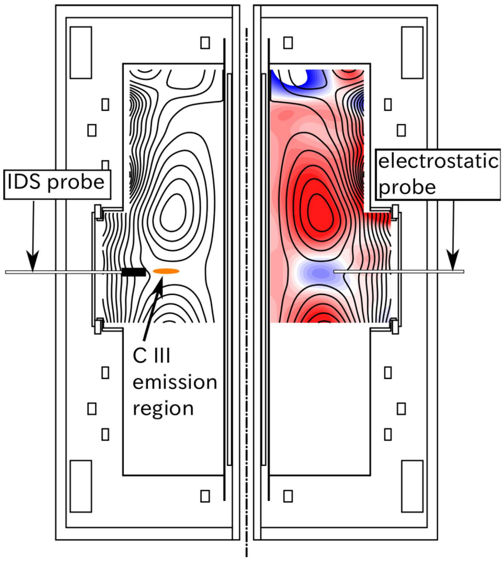

Fig. 3 Layout of electrostatic probe and IDS probe.

ion temperature.

5. Results and Discussion

Figure 4 shows r-z profiles of the poloidal flux and toroidal current density and radial profile of the floating potential. Measurement area of the floating potential is shown as blue two-way arrow on line/color contour plot.

This figure indicates that the floating potential is uniform across the current sheet at 200 µsec. After this time floating potential suddenly form a steep gradient around $R = 0.35$ m, where the X-point is located around this time. The abrupt decrease of floating potential outside the X-point is due to charge non-neutrality just outside the X-point. This charge non-neutrality was caused by the difference between the electron and ion motions around the X-point, indicating that the evidence of the two-fluid (Hall) effect during reconnection.

Time evolutions of reconnection rate ($-(d\psi/dt)$) and toroidal current density ($-j_t$) at the X-point are shown in Fig. 5. Also, radial profiles of floating potential (ϕ_f) and radial electric field (E_r) at specific time are shown. From this figure, it can be noted that until 200 µs the reconnection rate is no higher than the half of the peak reconnection rate and the toroidal current density continues growing up. In this phase, the floating potential is almost uniform and no steepening appears and so radial electric field is almost uniform across the current sheet. After 200 µs, the reconnection rate rapidly grows up and come to its peak at 205 µs, on the other hand the toroidal current density decreases. We can see from this fugure that after 200 µs floating potential start to form a steep gradient around $R = 0.35$ m, i.e., around the X-point, and the radial electric field at $R = 0.35$ m suddenly starts to grow. The time evolution tendency of these quantities can be paraphrased as follows: the two-fluid effect suddenly shows up when the reconnection rate abruptly grows up and the current density gradually decreases. Also, this may indicate that two-fluid effect enhances reconnection rate.

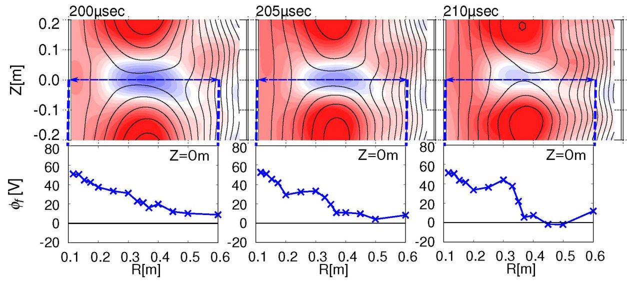

Fig. 4 2D profile of poloidal flux (line contour) and toroidal current density (color contour) and radial profile of floating potential ϕ_f.

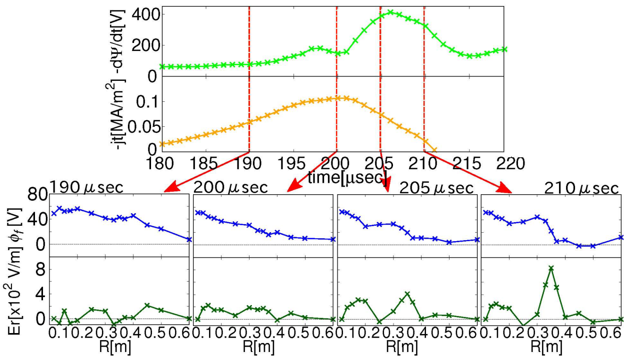

Fig. 5 Time evolutions of reconnection rate ($-(d\psi/dt)$) and toroidal current density ($-j_t$) at X-point, and radial profiles of floating potential (ϕ_f) and radial electric field (E_r) at t = 190, 200, 205 µsec.

Figure 6 shows the ion temperature at three radial positions together with r-z contours of the poloidal flux and toroidal current density, and the radial floating potential profile at 205 µs. Each signal from the IDS probe measurement is a line integrated emission from $R = 0.1$ m to the measurement position, and each measurement region of the IDS probe is denoted with black two-way arrow both on contour plots of ψ and j_t and radial profile plot of ϕ_f. From the IDS probe measurement data in Fig. 6, radial flow as fast as $V_i/V_A \sim 1$ is detected at $R = 0.36$ m, 0.46 m, where the X-point is included within the measurement area, while no ion flow is observed at $R = 0.26$ m, where the X-point is not included. The ion temperature is much higher after the completion of the ST formation. The ion temperature measured at $R = 0.26$ m is higher than that right after the ST formation but is still lower than that measured from the other positions. However, the fitted Gaussian may contain the effect of bulk motions arond the X-point. There exist strong flow around and outside the X-point and also there may occur ion heating around the X-point.

The floating potential measurement indicates that the

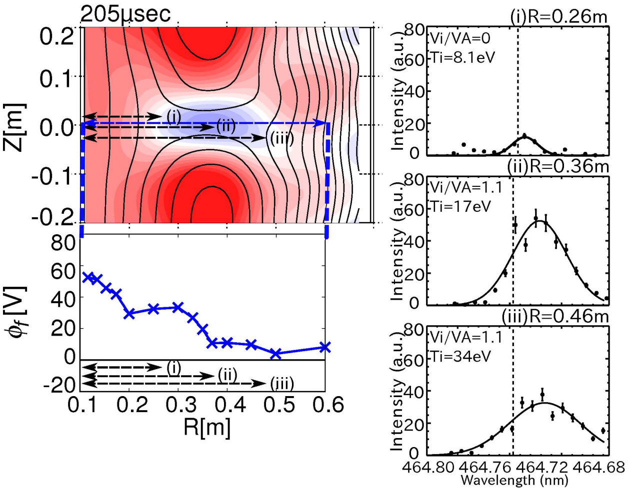

Fig. 6 The poloidal flux contour, floating potential profile and HeII line spectrums at three radial positions. The dashed line denote the center of the HeII line. The ion velocity is normalized by the poloidal Alfvénspeed of 24 km/s.

potential drop outside the X-point accelerate ions, causing ion heating around the X-point. In the UTST merging experiment, merging poloidal magnetic field B_p and toroidal megnetic field B_t are typically 0.01 T and 0.1 T, respectively, therefore the C^{2+} gyration period is $\tau_{Cc} = 3.9\,\mu s$ and the gyroradius is $\rho_C \sim 16$ mm. The acceleration time is roughly calculated as follows: From the potential gradient calculation in Fig. 5, the electrostatic electric field is estimated as $400 < E_r < 800$ V/m. The acceleration time τ_{acc} is calculated as follows.

$$\tau_{acc} = \frac{V_i m_i}{q E_r}, \tag{5}$$

where V_i is the ion velocity $V_i \sim 27$ km/s, q is the charge value of C^{2+}, which is $q = 3.2 \times 10^{-19}$ C, m_i is the mass of C^{2+} so $m_i = 2.0 \times 10^{-26}$ kg. Therefore, the acceleration time τ_{acc} is $2.1 < \tau_{acc} < 4.2\,\mu s$. The acceleration time can be less than the gyration period of C^{2+}, i.e., it is possible for C^{2+} to be accelerated up to 27 km/s only by the radial electric field. The possible thermalization mechanisms for accelerated ions are the remagnetization in the high-field downstream area and/or their collision in the downstream area with density pileup or fast shock [7]. Accelerated ions are magnetized in the downstream region, converting ion flow energy to thermal energy. The downstream region has density pileup and/or fast shock. When the ions accelerated into this region, fast shock increases collisions, thermalizing ions.

6. Conclusion

Radial profile of floating potential was measured for the first time by the electrostatic probe during magnetic reconnection in the UTST. When the reconnection rate increases the sudden floating potential drop was observed outside the X-point, as an evidence of two-fluid effect. This potential drop forms steep potential gradient around the X-point, increasing the C^{2+} outflow to $V_i/V_A \sim 1$. This potential drop also causes ion heating around the X-point through some ion dumping mechanism. The possible dumping mechanisms are their remagnetization and/or their collision in the downstream area with density pileup/fast shock.

Acknowledgements

This work was supported in partial by Grant-in-Aid for Scientific Research (KAKENHI) 22246119, 22686085, 25820434 and JSPS Core-to-Core Program 22001.

[1] Y-K.M. Peng and D.J. Strickler, Nucl. Fusion **26**, 769 (1986).
[2] A. Sykes *et al.*, Nucl. Fusion **41**, 1423 (2001).
[3] Y. Ono *et al.*, Fusion energy 2008 (IAEA Vienna, 2009, in DVD-ROM) EX/P9-4.
[4] T. Yamada *et al.*, in *Proc. 39th EPS Conf. on Plasma Physics and 16th Intl. Congress on Plasma Physics*, P1.013 (Stockholm, Sweden, July 2–6, 2012).
[5] M. Yamada *et al.*, Phys. Plasmas **13**, 052119 (2006).
[6] S. Kamio *et al.*, IEEJ Trans. FM, Vol.132, No.1, in press (2012).
[7] Y. Ono, H. Tanabe *et al.*, Phys. Rev. Lett. **18**, 185001, (2011).